JOURNAL OF MATERIALS SCIENCE 19 (1984) 3173–3184

Influence of impurities, such as carbon and sulphur, on the high temperature oxidation behaviour of $Fe_{72}Cr_{23}Al_5$ alloys

G. BEN ABDERRAZIK, G. MOULIN, A. M. HUNTZ
Laboratoire de Métallurgie Physique, LA no. 177, Université Paris XI, 91405 Orsay Cedex, France

R. BERNERON
Département Surfaces-Analyses Chimiques, IRSID, St Germain en Laye, France

Kinetic and analytical study of oxidation behaviour of $Fe_{72}Cr_{23}Al_5$ alloy in relation to the microstructure, particularly carbon and sulphur localization and chemical state, indicates that these elements have a strong influence on alumina growth and adherence. Competition between oxidation and a carbide precipitation slightly increases the oxidation rate during isothermal treatments but has a beneficial influence on the oxide scale adherence. Sulphide precipitation in the metallic substrate has a disastrous effect on oxidation: large weight gains are observed, due to internal oxidation at sulphides and presence of sulphur in the alumina. Moreover, it was confirmed that alumina growth is controlled by preferential oxygen diffusion along short-circuit paths.

1. Introduction

Corrosion studies on Fe–Cr–Al alloy (used for furnace resistors) have been carried out, up to now, by several authors [1–6]. This alloy develops, by oxidation, a protective scale of Al_2O_3 and consequently, must have a good oxidation resistance at high temperature. Nevertheless, when it is submitted to cyclic oxidation treatments in industrial furnaces, adherence losses are observed which induce disastrous damage of the oxidized Fe–Cr–Al alloy. Moreover, alloy impurities, such as carbon and sulphur, whose presence results either from the purity of starting materials, or from voluntary additions (carbon case) or atmosphere aggression during heat-treatments (sulphur case), can notably modify the oxidation resistance of this alloy.

The aim of this present study* is to establish the oxidation mechanism of Fe–Cr–Al alloy, taking into account its metallurgical history, and, in consequence, to explain the individual role of carbon and sulphur. The influences of carbon and sulphur on oxidation phenomena will be considered under several aspects: kinetic, microstructural and analytical, but also through diffusion properties and adherence alteration of the oxide scale, in order to be able, on a fundamental point of view, with the help of bibliographic data, to determine influence of carbon and sulphur on the oxidation mechanism of $Fe_{72}Cr_{23}Al_5$ alloy.

2. Experimental procedure and materials

In order to approach oxidation phenomena from several points of view, many techniques (whose characteristics have been detailed previously on other papers) are utilized:

(a) Optical microscopy; for such observations, samples are mechanically polished (SiC paper to grade 1200, then diamond paste to 2 μm) and electrolytically etched in a bath made up of an aqueous solution of 40 vol% HNO_3 (room temperature, ~ 3 V, 15 sec).

(b) Scanning electron microscopy equipped with energy-dispersive X-ray analysis.

(c) Electron microprobe equipped with a ZAF

*This study is part of a collaborative concerted research led by the CEFRACOR group "Corrosion par les gaz chauds".

0022–2461/84 $03.00 + .12

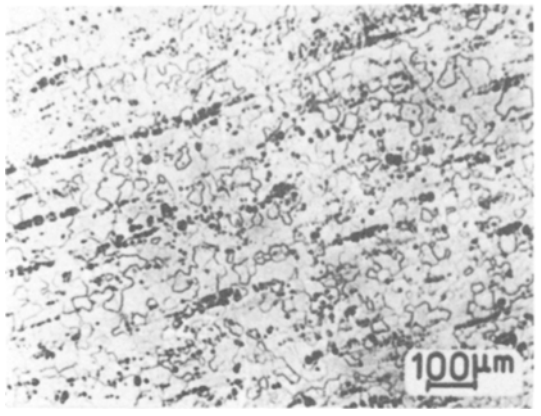

Figure 1 $Fe_{72}Cr_{23}Al_5$ microstructure after hot rolling.

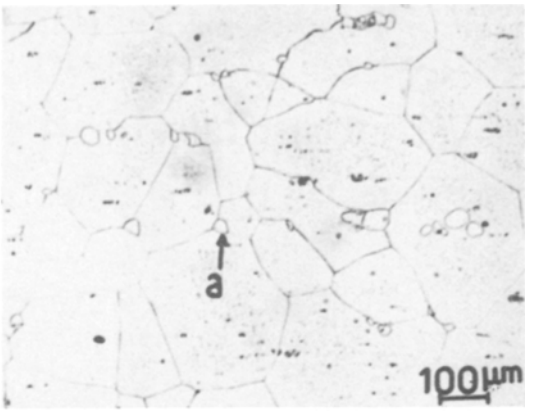

Figure 2 $Fe_{72}Cr_{23}Al_5$ microstructure after heat treatment (a) (48 h at 1000° C): precipitates of chromium carbide, ZrO_2 and $ZrCr_2$ (noted a →).

corrections programme in order to obtain quantitative values of element concentration.

(d) Glow discharge optical spectrometry (GDOS) [6].

(e) High resolution autoradiography based on use of radioactive tracers such as ^{14}C [7].

(f) Microthermogravimetry (Cahn thermobalance of high sensitivity: ± 2 µg).

(g) Heat treatments (described further).

The material tested is a $Fe_{72}Cr_{23}Al_5$ (proportions by weight) elaborated by Imphy S.A., hot-rolled down to 1.2 mm thickness and characterized by a grain size of about 20 µm. In such conditions, this ferritic alloy contains many precipitates enriched in chromium and carbon, or zirconium and oxygen, or aluminium and oxygen (composition determined by microprobe analysis). These precipitates have a preferential orientation along the rolling direction (Fig. 1). The composition of this alloy is given in Table I.

Several types of heat-treatments were carried out in order to obtain microstructures differing in terms of the nature and amount of precipitates and of the chemical state of the carbon (carbides or in solid solution):

(a) Heat-treatment (a) consisted of an anneal for 48 h at 1000° C under argon. Samples so treated were considered as standard and contained three types of precipitates (Fig. 2):

(i) chromium carbides mainly localized along grain boundaries. Some are observed in the grains.

(ii) zirconium oxide (ZrO_2).

(iii) $ZrCr_2$ phase.

The grain size is about 250 µm (Fig. 2).

(b) Heat-treatment (b) for 48 h at 1200° C under argon induced a good alloy homogenization, a stable grain size (~ 300 µm) (Fig. 3) and dissolution of chromium carbides and $ZrCr_2$ phase. After such a treatment, only zirconium oxide is observed along grain boundaries and in the grains (Fig. 3).

(c) Heat-treatment (c) for 48 h at 1200° C, then 24 h at 1000° C induced a stable grain size (~ 300 µm), chromium carbide precipitation and dissolution of $ZrCr_2$ phase (during the first step of this treatment) (Fig. 4).

All these treatments are followed by a rapid quench.

(d) Heat-treatment (d) consisted of a sulphidation treatment. The hot-rolled samples were previously heat-treated for 48 h at 1200° C, quenched, then sulphidized in controlled H_2/H_2S atmosphere apparatus [8] for 100 h at 800° C, with $P_{S_2} = 10^{-12}$ atm and $P_{H_2} = 0.4$ atm. After such a treatment, a sulphide gradient is observed from the sample surface to a depth of about 50 µm. In order to homogenize the sulphide distribution, samples are annealed, under argon, for 72 h at 1200° C. Fig. 5 shows that, under these conditions, sulphides are homogeneously localized in an area

TABLE I Elemental composition of $Fe_{72}Cr_{23}Al_5$ alloy

	C	Si	S	P	Mn	Cr	Al	Zr	Mg	Ca	Ni
Wt%	0.056	0.85	0.006	0.023	0.38	22.59	4.36	0.136	0.0045	0.009	0.35

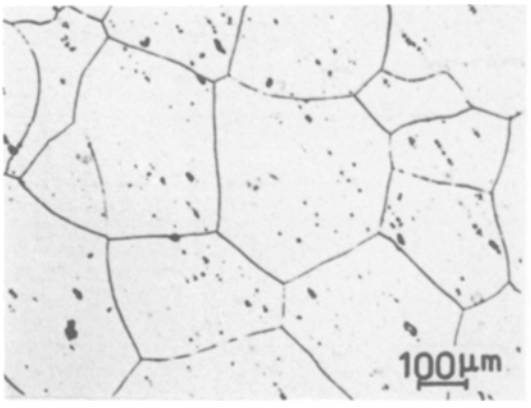

Figure 3 $Fe_{72}Cr_{23}Al_5$ microstructure after heat treatment (b) (48 h at 1200° C): precipitates consist of ZrO_2.

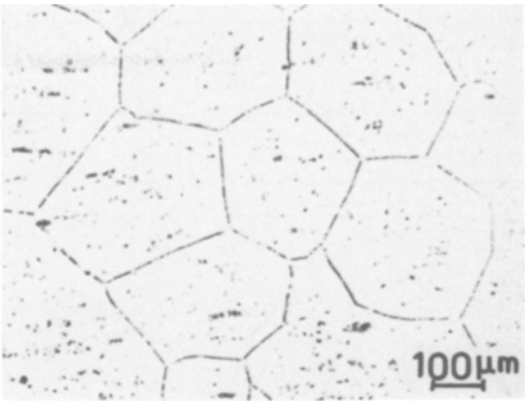

Figure 4 $Fe_{72}Cr_{23}Al_5$ microstructure after heat treatment (c) (48 h at 1200° C + 24 h at 1000° C): precipitates of chromium carbide and ZrO_2.

whose depth from the surface is about 250 µm. Chemical analyses* indicate that such samples contain 1.6 to 1.8 wt % S.

Oxidation of all samples was performed in a Cahn thermobalance under 1 atm of oxygen, with a flow of $2\,l\,h^{-1}$, between 900 and 1200° C. Before oxidation, samples were mechanically polished up to 2 µm diamond past. They were placed in the upper part of the thermobalance under oxygen flow and the pre-heated furnace was then positioned over the sample. Temperature stabilization was obtained in about 10 min.

Cyclic oxidation treatments were carried out in the same apparatus and under the same initial conditions. A cycle consisted of 20 h heat treatment (either at 900 or 1200° C), then cooling down to 250° C in about 4 h (300° C h^{-1} rate). For the next cycle, the upper temperature is reached also in about 4 h (heating rate = 300° C h^{-1}).

3. Experimental results

3.1. Oxidation kinetics aspect

When carbon is precipitated in samples (treatment (a)), classical phenomena are observed (Fig. 6): the higher the temperature, the faster the rate. For all oxidation temperatures, during an initial period, a large weight gain is observed, while the oxidation rate notably decreases during a second period. In all cases, parabolic oxidation laws are obtained (Fig. 7) after 1 to 4 h oxidation (the higher the temperature, the faster the beginning of the parabolic oxidation law). For oxidation

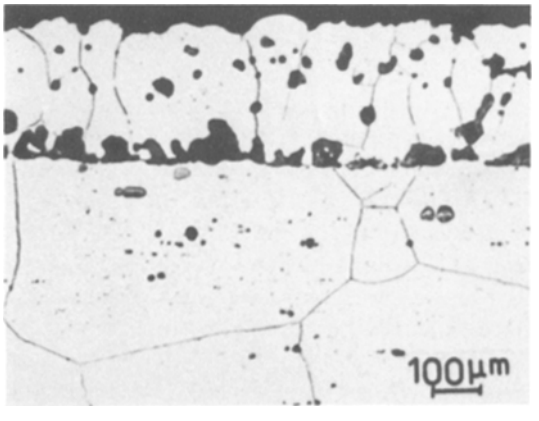

Figure 5 $Fe_{72}Cr_{23}Al_5$ after sulphidation (100 h at 800° C) and annealing at 1200° C (72 h). The upper zone (~ 250 µm) consists of a sulphidized area.

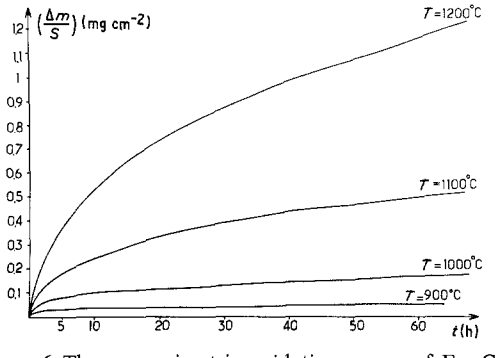

Figure 6 Thermogravimetric oxidation curves of Fe–Cr–Al samples pre-annealed at 1000° C, then oxidized under P_{O_2} = 1 atm.

*Chemical analyses were performed by M. Feillolay, IRSID.

TABLE II

		Samples (b) carbon in solid solution before oxidation	Samples (a) carbide precipitates before oxidation
Weight gain after 60 h	at 1100° C	0.38	0.50
Oxidation (mg cm^{-2})	at 1200° C	0.80	1.17

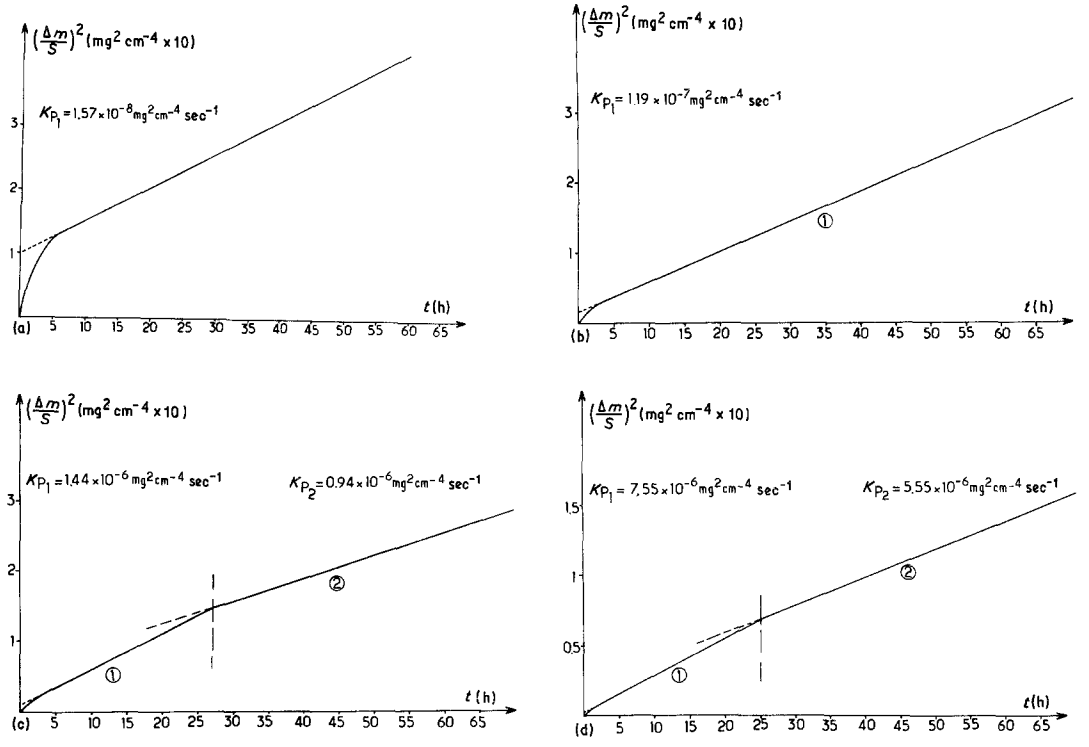

Figure 7 Parabolic plot of oxidation curves of Fe–Cr–Al samples pre-annealed at 1000° C: (a) oxidized at 900° C under $P_{O_2} = 1$ atm, (b) oxidized at 1000° C under $P_{O_2} = 1$ atm, (c) oxidized at 1100° C under $P_{O_2} = 1$ atm, and (d) oxidized at 1200° C under $P_{O_2} = 1$ atm.

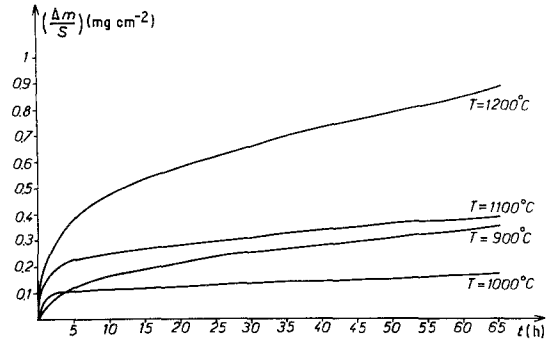

Figure 8 Thermogravimetric oxidation curves of Fe–Cr–Al samples pre-annealed at 1200° C, then oxidized under $P_{O_2} = 1$ atm.

at 1100 or 1200° C, two parabolic laws are successively noted, characterized by slightly different values of the parabolic constant k_p.*

When carbon is in solid solution in the samples (after treatment (b)), oxidation curves appear to be different from the previous case (Fig. 8). For oxidation from 1000 to 1200° C, the kinetic curves look like curves obtained for samples pre-annealed at 1000° C: during the first three hours, the weight gain is large, then followed by a low kinetic rate. When the alloy is oxidized at 900° C, a curious behaviour can be noted: the slackening of the oxidation rate, after some hours oxidation, is no longer observed. Consequently, the oxidation

*k_p is obtained from the law: $(\Delta m/S)^2 = k_p t + cte$

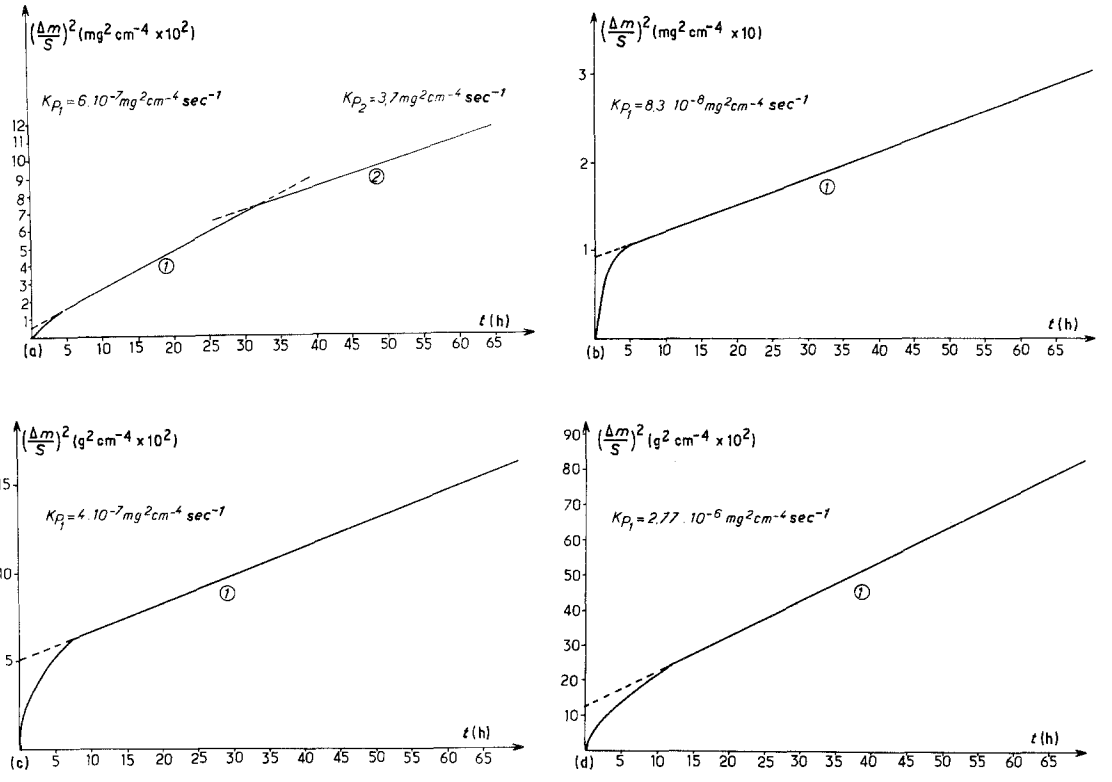

Figure 9 Parabolic plot of oxidation curves of Fe–Cr–Al samples pre-annealed at 1200° C: (a) oxidized at 900° C, under $P_{O_2} = 1$ atm, (b) oxidized at 1000° C, under $P_{O_2} = 1$ atm, (c) oxidized at 1100° C, under $P_{O_2} = 1$ atm, and (d) oxidized at 1200° C, under $P_{O_2} = 1$ atm.

weight gain for a sample oxidized at 900° C is higher than for a sample oxidized at 1000° C: for 65 h oxidation the weight gain is much the same as for a sample oxidized at 1100° C and would be higher for longer oxidation times. For all oxidation temperatures tested, the kinetics follow a parabolic law $(\Delta m/S)^2 = k_p t + k_0$, with two parabolic periods for a sample oxidized at 900° C (Fig. 9). It can be noted also, that, when the alloy is oxidized at 1000 to 1200° C, weight gains and oxidation rate of such samples (pre-annealed at 1200° C) are lower than for samples (a) (pre-annealed at 1000° C) where carbon is precipitated. For example, Table II shows some weight gain values.

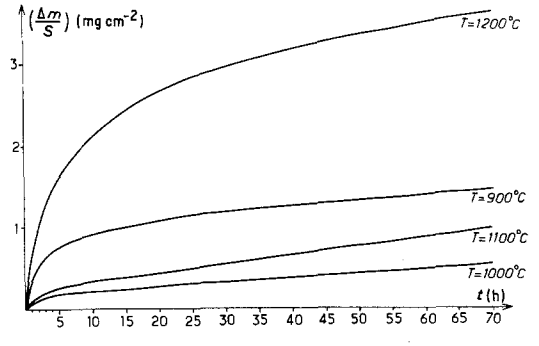

Figure 10 Thermogravimetric oxidation curves of Fe–Cr–Al samples pre-sulphidized, annealed at 1200° C, then oxidized under $P_{O_2} = 1$ atm.

When samples are previously sulphidized (treatment (d)), weight gains by oxidation are much larger than for samples without sulphides, about three times greater (Fig. 10). The curious behaviour of samples pre-annealed at 1200° C, then oxidized at 900° C, is always observed and amplified for a sulphidized alloy: in this case, the weight gain is higher than for samples oxidized at 1100° C. For such pre-sulphidized samples, the oxidation kinetics do not follow a parabolic law.

3.2. Analytical aspect

The concentration variations of heavy elements were more particularly studied by electron microprobe analyses, while optical spectrometry allowed the determination of the concentration variations of light elements, (giving simultaneously, information about other elements). Analyses were

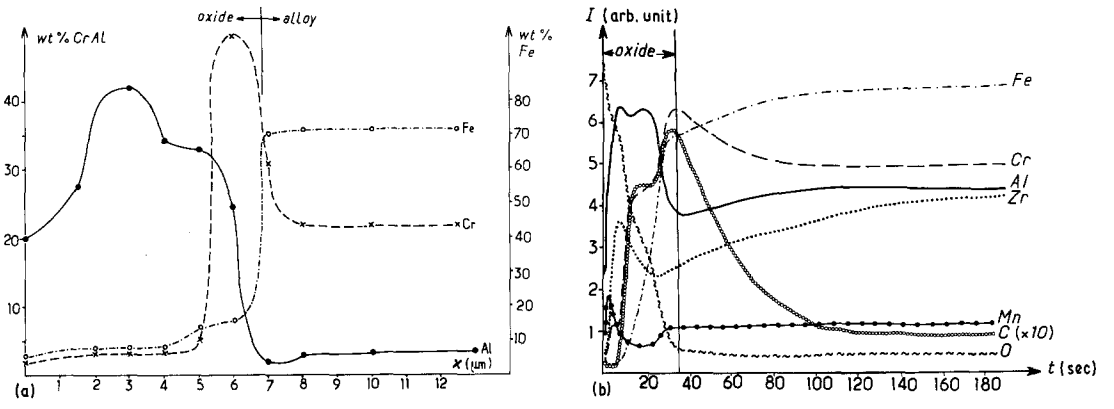

Figure 11 Concentration profiles of elements in alumina scale developed on FeCrAl pre-treated at 1200° C and oxidized at 900° C ((a) 70 h and (b) 22 h, respectively): (a) microprobe analysis, corrected values of concentration; (b) GDOS analysis.

carried out on the oxide scale and on the subjacent metallic substrate.

In the case of unsulphidized alloy, oxide scale obtained by corrosion in pure oxygen consists of alumina whatever the pre-annealing may be. Nevertheless, the purity of alumina scales depends on temperatures of both pre-annealing and oxidation treatment: so when pre-treated at 1200° C, then oxidized at 900° C, the alumina scale is enriched in chromium (~ 4%) and iron (~ 8%) (Fig. 11) and, at the metal–oxide interface, a chromium enrichment is observed.

Moreover, by optical spectrometry, it is possible to distinguish two cases according to the kind of the pre-treatment:

(i) when carbon is precipitated in the alloy before oxidation, (pre-treatment (a)), profiles obtained by GDOS do not show an preferential carbon localization at the oxide–metal interface (Figs. 12a and b) whatever may be the oxidation temperature.

(ii) when carbon is in solid solution in the alloy

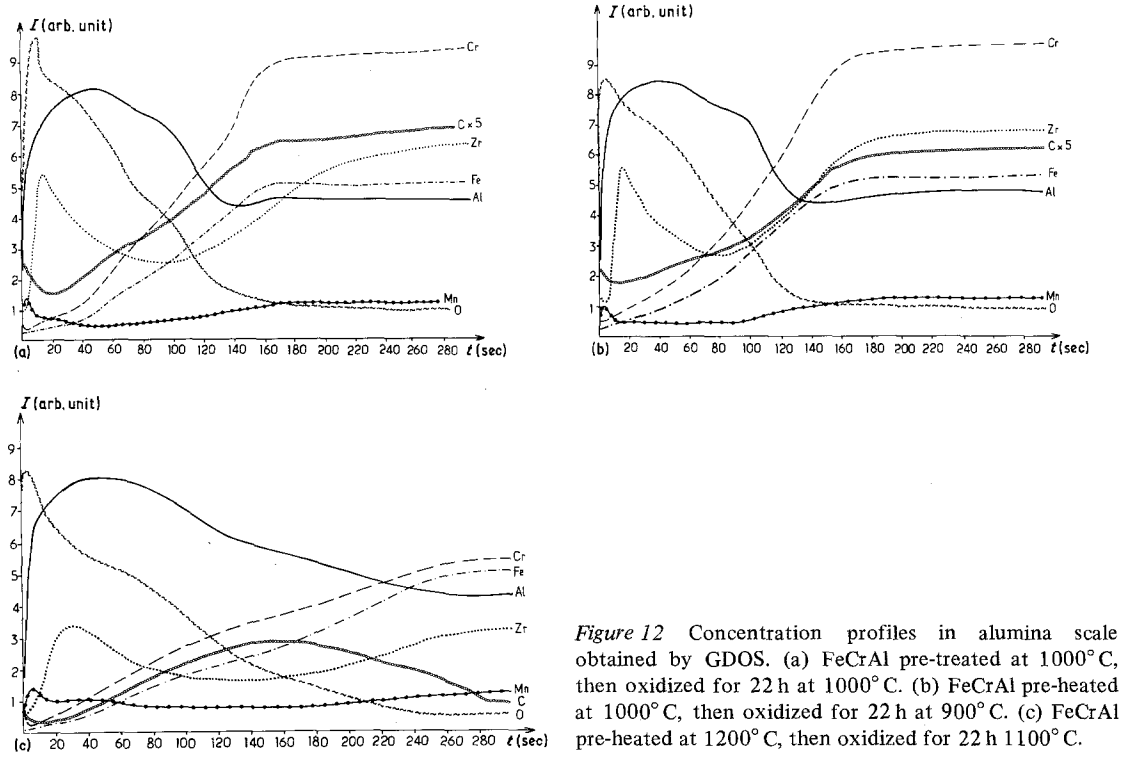

Figure 12 Concentration profiles in alumina scale obtained by GDOS. (a) FeCrAl pre-treated at 1000° C, then oxidized for 22 h at 1000° C. (b) FeCrAl pre-heated at 1000° C, then oxidized for 22 h at 900° C. (c) FeCrAl pre-heated at 1200° C, then oxidized for 22 h 1100° C.

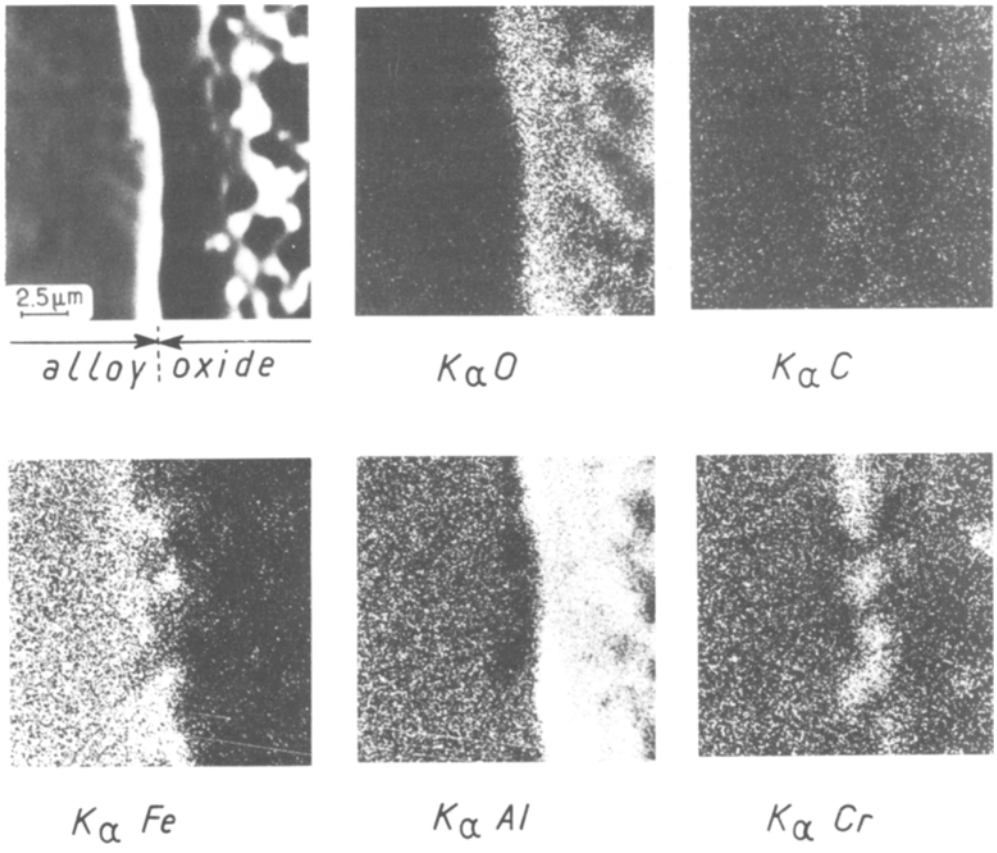

Figure 13 X-ray images of Fe–Cr–Al pre-treated at 1200° C and its oxide scale developed at 900° C. Oxidation time was 70 h.

before oxidation, (pre-treatment (b)), preferential carbon localization is observed at the oxide–metal interface (Fig. 12c). This high carbon concentration is associated with a chromium enrichment when oxidation is carried out at 900° C (see Fig. 11). Moreover, a second area, enriched in carbon appears in the alumina scale (Fig. 11b). Always for oxidation at 900° C, X-ray images (Fig. 13) show that a continuous layer enriched in carbon and chromium is located at the metal–oxide interface. It is never the case of other samples oxidized at 1000, 1100 or 1200° C (Fig. 14). These results about carbon segregation were confirmed by high resolution autoradiography (^{14}C being used as a tracer).

In the case of presulphidized samples (treatment (d)), an enrichment of chromium associated with a carbon preferential localization is always observed in the alumina scales, near the oxide–metal interface, whatever the oxidation temperature may be (Fig. 15). Moreover, a sulphur enrichment appears at the outer part of the oxide scale (Figs. 15b and 16a). Electronic microprobe profiles show oxide scale heterogeneities, (Fig. 16), particularly chromium enrichments associated with sulphur enrichments (Fig. 16a), located at the inner and outer parts of the oxide scale. When samples are oxidized at 900° C, chromium is rather preferentially localized at the metal–oxide interface. X-ray images (Fig. 17) confirm all these results and show selective internal oxidation on chromium sulphides in the metallic substrate.

4. Discussion

The parabolic laws observed for the oxidation kinetics of Fe–Cr–Al alloy indicate that alumina growth is controlled by diffusion processes which are thermally activated, according to the fact that k_p values follow an Arrhenius law, (Fig. 18), with an activation energy of about 300 kJ mol^{-1}, whatever the microstructural state of the alloy may be. Activation energy values of cationic and anionic diffusion in alumina are collected in Table III [9–14]. By comparison of these values

TABLE III Activation energies of diffusion in Al_2O_3

Diffusing elements	Q (kJ mol^{-1})	Diffusion process	References
Al	476	Lattice (intrinsic vacancies)	[9]
Cations such as Cr, Fe, Ni	250 to 300	Lattice (extrinsic vacancies)	[10]
O	600 to 800	Lattice	[11–14]
O	~ 460	Grain boundaries and lattice	[11]

and our value of 300 kJ mol^{-1} obtained by oxidation experiments, it can be assumed that alumina growth is controlled either by aluminium diffusion by extrinsic vacancies, or by oxygen diffusion by short-circuit paths. Taking into account that alumina developed on metallic substrates proceeds by inward growth [1, 15–17], it can be concluded that alumina growth on Fe–Cr–Al alloy is induced by prevailing oxygen diffusion by short-circuit paths, such as grain boundaries, microcracks and porosities.

On the basis of the kinetics results obtained in this study (Figs. 7, 9 and 18), two remarks can be developed; one concerning the fact that two parabolic laws are obtained according to the chemical state of carbon; the other related to the curious oxidation behaviour of the samples pre-treated at 1200° C and oxidized at 900° C:

(a) Two distinct parabolic laws are observed for oxidation at $T > 1000°$ C when the pre-treatment has induced carbide precipitation (Fig. 18a), and for oxidation at $T \leqslant 1000°$ C when the pre-treatment has induced dissolution of carbides (Fig. 18b). These observations show the important influence of the carbon state and localization in the metallic substrate, taking into account the fairly constant size of sample grains, whatever the previous heat-treatment may be. Thus, for samples pre-treated to favour carbide precipitation, further oxidation at 1100 or 1200° C progressively induces dissolution of carbides. This modifies the nature and amount of defects and consequently

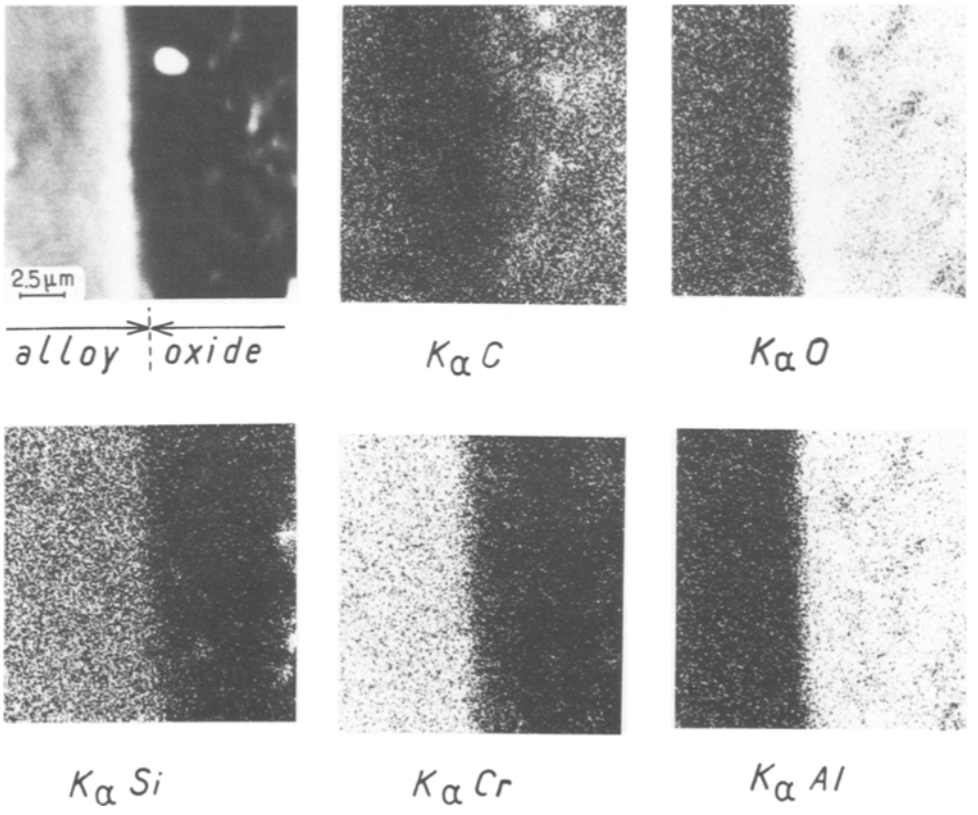

Figure 14 X-ray images of Fe–Cr–Al pre-treated at 1000° C and its oxide scale developed at 900° C.

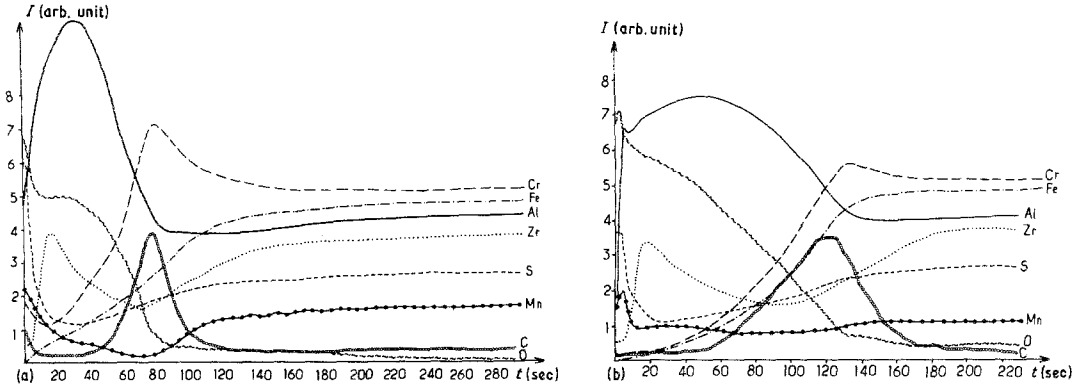

Figure 15 Concentration profiles, (obtained by optical spectrometry), of elements in alumina scale developed on pre-sulphidized Fe–Cr–Al samples annealed at 1200° C: (a) oxidation for 22 h at 1200° C; (b) oxidation for 22 h at 900° C.

the oxidation rate, that is the k_p value. For samples with carbon in solid solution, further oxidation at 900 or 1000° C induces carbide precipitation; thus, after some hours oxidation, changes in amount and nature of defects appear. It can be noted that the carbide precipitation at the oxide–metal interface decreases the alumina growth rate. It was verified, (by dilatometric tests), that this dissolution, or precipitation, of carbides appears at about 1000° C and extends over some hours, thus leading to modification of the oxidation kinetics during a first period.

(b) The curious behaviour of samples pre-treated at 1200° C, then oxidized at 900° C, (cf. Fig. 8), can be interpreted on the basis of competition between oxidation and carbide precipitation. Carbides homogeneously and progressively precipitate in all the matrix of the metallic substrate and in the oxide scale. Carbides present in the oxide scale subsequently react with oxygen in order to induce either chromium oxi-carbides or chromium oxide Cr_2O_3. These phenomena induce an important weight gain and an enrichment of the oxide scale in chromium and carbon. If oxidation is carried out at other temperatures, for example 1000° C, carbide precipitation is retarded and begins when chromium and iron gradients in the matrix have already been induced by alumina growth. In such conditions, the driving power for precipitation is important and provokes a coarse precipitation at the oxide–metal interface which decreases the diffusion rate and, consequently, the alumina growth rate. Such assumptions are confirmed by analysis results, (cf. Fig. 12), which show an enrichment in carbon at the oxide–metal interface.

Nevertheless, carbon influence must be balanced by the possible role of other impurities, such as zirconium, which is also observed in the oxide scale (cf. Figs. 11 and 12). Moreover, supplementary oxidation experiments, carried out at 900° C (Fig. 19), indicate that oxidation kinetics depend

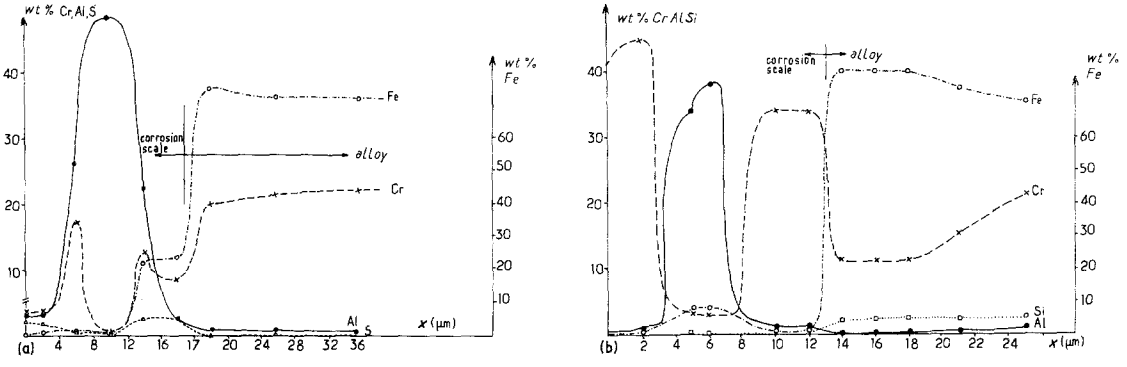

Figure 16 Concentration profiles (microprobe analysis) of elements in alumina scale of pre-sulphidized Fe–Cr–Al samples annealed at 1200° C: (a) oxidized for 70 h at 1200° C; (b) oxidized for 70 h at 900° C.

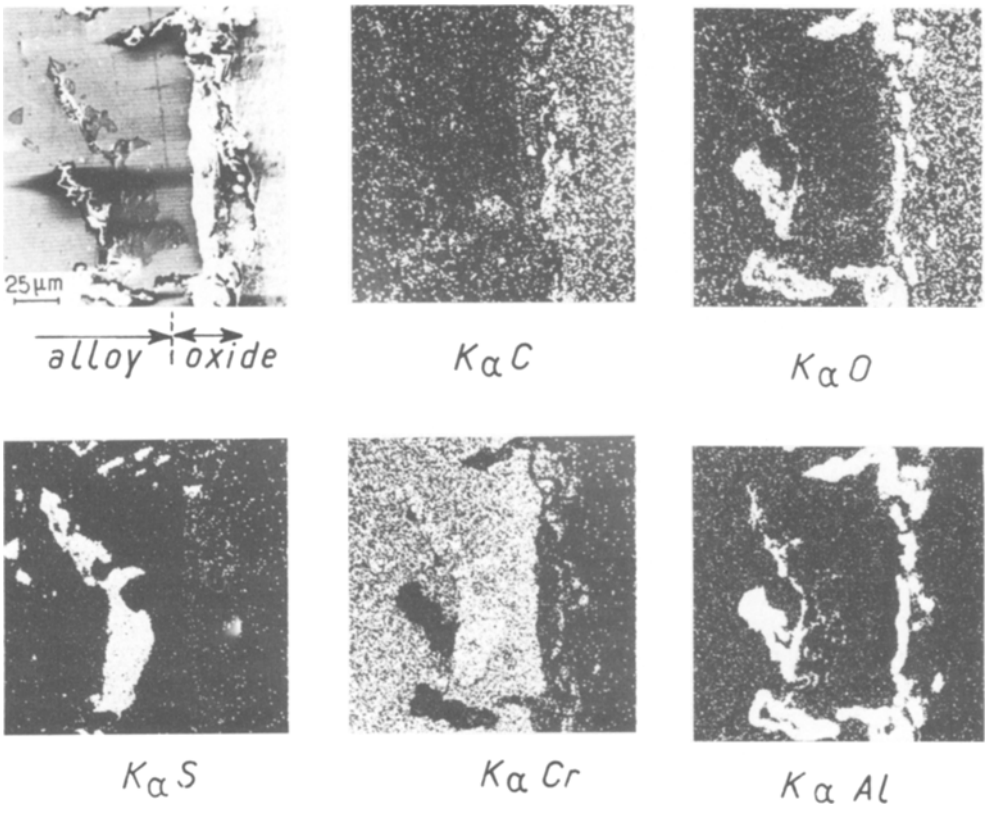

Figure 17 X-ray images of Fe–Cr–Al sulphidized, then pre-treated at 1200° C and oxidized for 70 h at 1200° C.

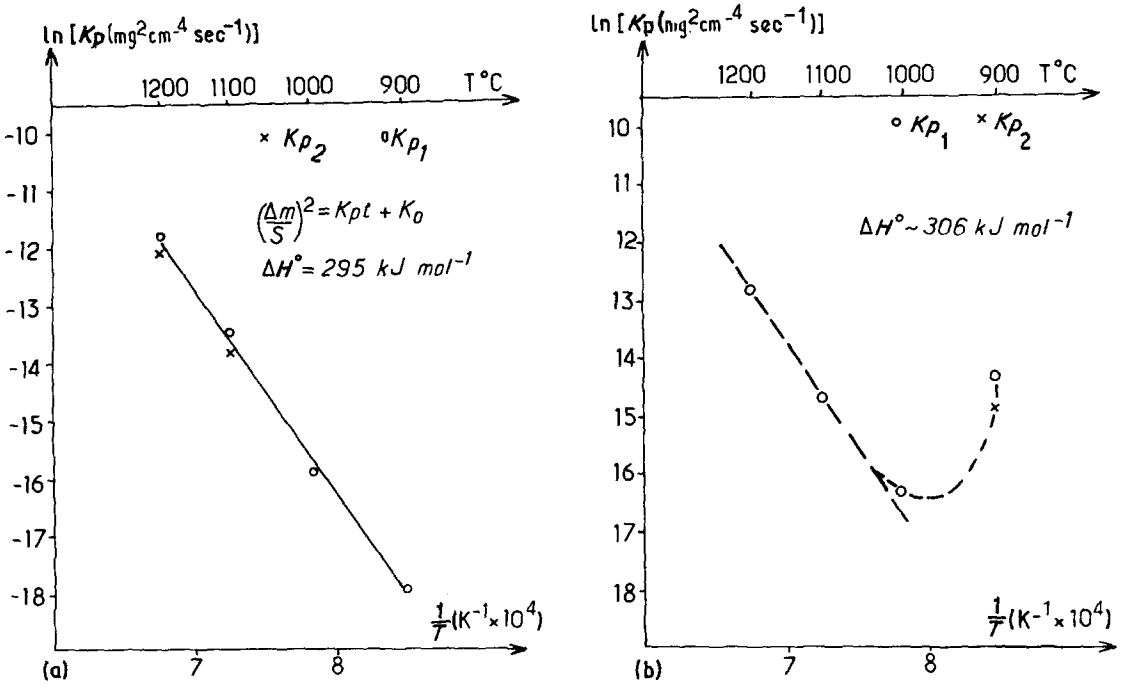

Figure 18 Arrhenius plot of parabolic oxidation constant of FeCrAl: (a) pre-treated at 1000° C and then oxidized under $P_{O_2} = 1$ atm, (b) pre-treated at 1200° C, then oxidized under $P_{O_2} = 1$ atm.

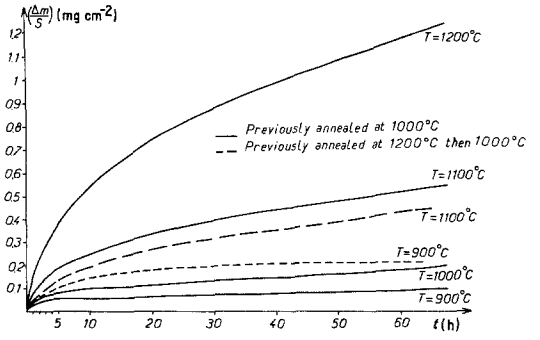

Figure 19 Thermogravimetric oxidation curves of Fe–Cr–Al samples with different treatments. $P_{O_2} = 1$ atm.

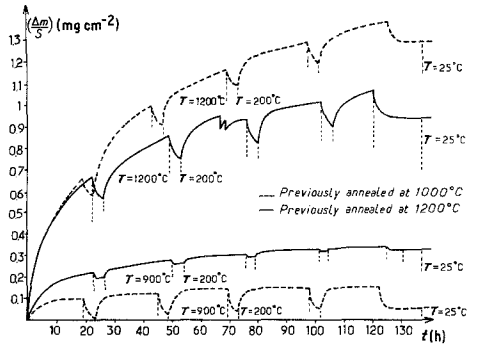

Figure 20 Thermogravimetric curves obtained by cyclic oxidation treatments for different Fe–Cr–Al samples. $P_{O_2} = 1$ atm.

on carbon and zirconium chemical state. Indeed, zirconium can be either in solid solution (pre-treatment at 1200° C) or precipitated ($ZrCr_2$ second phase when the pre-treatment is carried out at 1000° C). Thus, by comparison of the two curves obtained by oxidation at 900° C, (Fig. 19), it can be noted that a pre-treatment at 1000° C ($ZrCr_2$ presence) induces an oxidation rate slower than for samples pre-treated at 1200° C, then 1000° C (dissolution of $ZrCr_2$ phase during the first treatment at 1200° C). So, zirconium in solid solution increases the oxidation rate of Fe–Cr–Al alloy, probably on account of its effect on alumina defects due to its valences state (Zr^{4+}) [18].

All the preceding remarks about carbon state and localization must be taken into account when considering problems of the oxide scale adherence on the metallic substrate. When carbides precipitate in the metallic matrix as soon as oxidation begins, (for example pre-treatment at 1200° C and oxidation at 900° C), then the adherence of the oxide scale is improved (Fig. 20); in such a case, during cyclic oxidation treatments the weight loss during cooling is notably decreased.

Besides, this study shows the important influence of sulphur on the oxidation behaviour of Fe–Cr–Al alloy. Sulphur modifies the oxidation kinetics and the oxide scale composition. Firstly, an internal oxidation on sulphides in the metallic substrate appears: sulphides are decomposed with formation of chromium oxide Cr_2O_3. Such a reaction is induced at the beginning of oxidation processes and is going on during all the oxidation cycle, so that no parabolic law can be obtained [19–21]. Moreover, sulphide presence induces modifications of the oxide scale: during inward growth of alumina, some chromium sulphides are included in the oxide scale. Thus, near the oxide–metal interface, either simultaneous enrichment in sulphur and chromium, (Figs. 15 and 16), are locally observed and are due to undecomposed sulphides, or only enrichment in chromium appears and indicates that sulphides included in the scale have reacted with oxygen in order to give Cr_2O_3. Near the oxide–gas interface, enrichments in chromium and sulphur are observed (Figs. 15 and 16), due to the sulphide decomposition and to sulphur outward diffusion according to the instability of sulphur in alumina [22]. Such phenomena and, more particularly chromium and sulphur presence in alumina, modify the nature and concentration of defects in alumina and consequently the growth rate of this oxide. The two parameters, internal oxidation and modification of alumina defects, induce an important weight gain when compared to alloy without sulphides. In order to point out the respective influence of these two parameters and the role of impurities on alumina defects, experiments of corrosion in electric fields and analyses by EXAFS are actually carried out.

5. Conclusion

During oxidation of Fe–Cr–Al, a protective alumina scale is developed by inward growth. For all temperatures tested, parabolic kinetic laws are observed. In most cases, two oxidation periods appear with slightly different parabolic constant values. Oxidation process is thermally activated, according to an Arrhenius law, with an activation energy of about 300 kJ mol^{-1}, whatever the microstructural state of the alloy may be. Growth mechanism is explained by preponderant diffusion of oxygen along short-circuit paths.

The chemical state of carbon, in solid solution

or precipitated, has a notable influence on oxidation behaviour of Fe–Cr–Al alloy. When carbon is in solid solution in the metallic matrix, further oxidation at temperatures higher than 900° C induces coarse precipitation of carbides at the oxide–metal interface, which decreases the oxidation rate. In return, if oxidation is carried out at 900° C, carbide precipitation occurs progressively and simultaneously to oxidation; then some carbides are included in alumina and react with oxygen; these phenomena explain that the oxidation kinetic is increased and the oxide scale composition modified. Progressive precipitation of carbides also improves the oxide scale adherence on the metallic substrate.

Other impurities, such as zirconium, also have an influence, Particularly, zirconium in solid solution increases the oxidation rate of Fe–Cr–Al alloy.

The influence of sulphur on Fe–Cr–Al oxidation is rather disastrous: the important weight gains are due to internal oxidation on sulphides present in the metallic substrate and to the inclusions of some sulphides in the oxide scale, which may react with oxygen, thus inducing enrichment of alumina in chromium and sulphur; further oxidation of chromium and defects created by the presence of sulphur increase the alumina growth rate. It must be noted that sulphur is unstable in alumina and diffuses towards the oxide–gas interface. The complexity of the phenomena explains that the oxidation kinetic laws are no longer parabolic.

References

1. D. P. WHITTLE and J. H. STRINGER, *Phil. Trans. R. Soc. Lond.* **A295** (1980) 309.
2. M. LOUDJANI, J. C. PIVIN, C. ROQUES-CARMES, J. H. DAVIDSON and P. LACOMBE, *Met. Trans. A* **13** (1982) 1299.
3. D. DELAUNAY, Doctor Ingenior Thesis, Université Paris-Sud, Orsay (1980).
4. J. C. COLSON, M. LAMBERTIN and J. P. LARPIN, *Mem. Sci. Rev. Met.* (1977) 687.
5. J. LIONS, J. P. TROTTIER and M. FOUCAULT, *ibid.* (1980) 743.
6. B. ALEXANDRE, R. BERNERON, J. C. CHARBONNIER, R. NAMDAR-IRANI and L. NEVOT, *ibid.* (1981) 483.
7. G. V. PRABHU GAUNKAR and A. M. HUNTZ, *Int. J. Appl. Rad. Isotopes* **30** (1979) 601, 761.
8. G. MOULIN, M. AUCOUTURIER and P. LACOMBE, *J. Nucl. Mater.* **82** (1979) 347.
9. A. E. PALADINO and W. D. KINGERY, *J. Chem. Phys.* **37** (5) (1962) 957.
10. B. LESAGE, A. M. HUNTZ and G. PETOT-ERVAS, *Rad. Eff.* **75-555** (1983) 283.
11. Y. OISHI and W. D. KINGERY, *J. Chem. Phys.* **33** (1960) 480.
12. K. P. R. REDDY and A. R. COOPER, *Amer. Ceram. Soc. Bull.* **55**(4) (1976) 402.
13. D. J. REED and B. J. WUENSCH, *ibid.* **63** (1) (1980) 88.
14. P. L. ANDERSON, Thesis MIT (1967).
15. R. R. DILS and P. S. FOLLANSBEE, Pratt and Whitney Aircraft Report 74-005 (1974).
16. J. STRINGER, "Non-Stoichiometry, Diffusion and Electrical Conductivity in Binary Metal Oxides", edited by P. Kofstad (Wiley, New York, NY, 1972).
17. F. A. GOLIGHTLY, F. H. STOTT and G. C. WOOD, *Oxid. Met.* **10** (1976) 163.
18. K. P. R. REDDY, J. L. SMIALEK and A. R. COOPER, *ibid.* **17** (1982) 429.
19. G. MOULIN, Doctor Thesis, Université Paris-Sud Orsay (1981), and Metaux Corrosion Industrie 687-688 (1982) 361, 689 (1983) 1.
20. J. C. COLSON, D. DELAFOSSE and P. BARRET, *Bull. Soc. Chim. France* **1** (1968) 146.
21. G. MARTIN, "Solid State Phase Transformations in Metals and Alloys" (Les éditions de la Physique, ecole d'Eté d'Aussois, 1978).
22. M. LOUDJANI, private communication (1983).

Received 29 September
and accepted 11 October 1983